The Canyon Diablo impact event: Projectile motion through the atmosphere

Natalia ARTEMIEVA[1, 2*] and Elisabetta PIERAZZO[2]

[1]Institute for Dynamics of Geospheres, Russian Academy of Science Leninsky pr. 38, bldg.1, Moscow 119334, Russia
[2]Planetary Science Institute, 1700 E. Ft. Lowell, Suite 106, Tucson, Arizona 85719–2395, USA
*Corresponding author. E-mail: artemeva@psi.edu

Abstract–Meteor Crater is one of the first impact structures systematically studied on Earth. Its location in arid northern Arizona has been ideal for the preservation of the structure and the surviving meteoric material. The recovery of a large amount of meteoritic material in and around the crater has allowed a rough reconstruction of the impact event: an iron object 50 m in diameter impacted the Earth's surface after breaking up in the atmosphere. The details of the disruption, however, are still debated. The final crater morphology (deep, bowl-shaped crater) rules out the formation of the crater by an open or dispersed swarm of fragments, in which the ratio of swarm radius to initial projectile radius C_d is larger than 3 (the final crater results from the sum of the craters formed by individual fragments). On the other hand, the lack of significant impact melt in the crater has been used to suggest that the impactor was slowed down to 12 km/s by the atmosphere, implying significant fragmentation and fragments' separation up to 4 initial radii. This paper focuses on the problem of entry and motion through the atmosphere for a possible Canyon Diablo impactor as a first but necessary step for constraining the initial conditions of the impact event which created Meteor Crater. After evaluating typical models used to investigate meteoroid disruption, such as the pancake and separated fragment models, we have carried out a series of hydrodynamic simulations using the 3D code SOVA to model the impactor flight through the atmosphere, both as a continuum object and a disrupted swarm.

Our results indicate that the most probable pre-atmospheric mass of the Meteor Crater projectile was in the range of $4 \cdot 10^8$ to $1.2 \cdot 10^9$ kg (equivalent to a sphere 46–66 m in diameter). During the entry process the projectile lost probably 30% to 70% of its mass, mainly because of mechanical ablation and gross fragmentation. Even in the case of a tight swarm of particles ($C_d < 3$), small fragments can separate from the crater-forming swarm and land on the plains (tens of km away from the crater) as individual meteorites. Starting from an impactor pre-atmospheric velocity of ~18 km/s, which represents an average value for Earth-crossing asteroids, we find that after disruption, the most probable impact velocity at the Earth's surface for a tight swarm is around 15 km/s or higher. A highly dispersed swarm would result in a much stronger deceleration of the fragments but would produce a final crater much shallower than observed at Meteor Crater.

INTRODUCTION

Barringer Meteorite Crater, normally referred to as Meteor Crater, is located about 35 miles (55 km) east of Flagstaff near the southern edge of the Colorado Plateau, in the northern Arizona grassland (USA). It is a simple, bowl-shaped crater about 1.2 km in diameter and 170–200 m deep, surrounded by a 40–50 m high rim (e.g., Kring 2007). Seen from above, the crater has a "squarish" shape caused by the presence in the region of two mutually perpendicular sets of vertical joints of uniform strike (e.g., Shoemaker 1963). The age of the structure has been estimated at approximately 49,000 yr, based on

thermoluminescence (Sutton 1985) and cosmogenic nuclides (^{36}Cl and ^{14}C, Phillips et al. 1991; ^{10}Be and ^{26}Al, Nishiizumi et al. 1991) studies.

The crater was formed by a relatively small iron impactor and is associated with hundreds of iron meteorites that have been recovered around the crater since the late 1800s. Its unusual appearance attracted much attention and early speculations on its extraterrestrial origin at a time when impact cratering was not considered a geologic process. As a result, it can be safely said that the early studies of Meteor Crater paved the way for the understanding of impact cratering and its incorporation among the important

geological processes that shape the solid surfaces of planetary objects.

Since the very early studies of Meteor Crater, it has been hypothesized that the crater was formed by the impact of a meteorite swarm (Barringer 1909; Moulton 1929; Nininger 1956). However, none of the numerical studies of the crater formation that followed took into account the possible atmospheric disruption of the Canyon Diablo projectile (Bjork 1961; Bryan et al. 1978; Roddy et al. 1980; Schnabel et al. 1999). Recently, simple atmospheric entry models for an iron meteorite similar to Canyon Diablo have been used to suggest the impacting object must have broken up and decelerated substantially during its travel through the atmosphere. The largest fragment reaching the ground may have had an impact speed as low as 12 km/s (Melosh and Collins 2005), not the 15–30 km/s generally assumed in numerical impact models of the event. Smaller fragments would reach the surface at much lower velocities. This lower impact velocity has thus been used to explain the lack of substantial impact melt recovered in and around the crater, which was originally attributed to presence of volatiles in the target (Kieffer and Simonds 1980; Hörz et al. 2002).

In this paper, we address in detail the problem of entry and motion through the atmosphere for a Canyon Diablo projectile. We will start with simplified analytical models routinely used to address disruption, and end with a full-scale three-dimensional simulation of the entry process. This is the first step to a more accurate modeling of the Canyon Diablo impact, necessary for constraining the initial conditions of the impact event that created Meteor Crater, and for understanding the dispersion of impactor material on the surrounding plains.

The Fate of the Impactor—Findings and Geochemistry

A detailed description of Barringer Meteorite Crater and references to the papers about the history of its exploration may be found in a recently published extensive field guide (Kring 2007). In this section, we discuss briefly early ideas about the projectile and its distribution around the crater.

The nature of the impacting body, whether a solid mass or a swarm, was discussed since the early 1900s. In his 1909 paper, Barringer described the impactor to be a swarm of objects, with a heavy central mass (or masses) responsible for the formation of the crater. This was a change from earlier assumptions of the impactor being a single solid mass. Moulton went as far as hypothesizing that the impacting swarm was in the shape of a thin disk, 2,000 to 3,000 feet (600–900 m) in diameter (Moulton 1929). Barringer also provided a detailed map (e.g., see Kring 2007, Fig. 8.1) showing the distribution of meteoritic material, Canyon Diablo irons and shale balls, collected and documented at that time (it obviously does not include meteoritic material removed by occasional visitors of the area and/or Native

American Indians living in the area before the white settlement). Later Nininger concluded that Barringer's shale balls were pieces of impactor that were heated to temperatures above about 800 °C (Nininger 1956). In particular, Nininger focused on the smaller material, metallic spheroids and similar particles that seem to make up the bulk of meteoritic material distributed around the crater. His work brought him to support the hypothesis that Meteor Crater and the Canyon Diablo irons were the results of the fragmentation of a heterogeneous body.

Below is a list of the various materials identified over the years as constituting or containing mostly impactor material:

1. *Canyon Diablo meteorites*: the more obvious pieces of impactor; they litter the region surrounding the crater. By the early 1900s, thousands of irons were collected within a radius of 5.5 miles from the crater with increasing abundance towards the crater (e.g., Barringer 1909). As early as 1908 G.P. Merrill estimated that since their first identification in 1891 up to 20,000 kg of Canyon Diablo iron meteorites, ranging from less than 25 g to more than 500 kg in weight, had been already collected in the area surrounding Meteor Crater (Merrill 1908). However, it is possible that a large number of irons was removed from the region unknowingly to Merrill. Nininger (1956) reported about rumors that several carloads of irons were shipped to a smelter in El Paso, Texas. Unfortunately, there is no way of knowing how many irons were recovered early on, nor where most of them were found. Based on the recorded findings, irons appear to be distributed more or less uniformly in the plains around the crater, while close to the crater and on the crater rim there is a strong concentration of irons in the northeast direction.

2. The Canyon Diablo meteorites are classified as octahedrite meteorites, whose major elements are Fe (89.7%), Ni (7.1%), and Co (0.4%) (e.g., Moore et al. 1967; Buchwald 1975b). Their mineralogy depends in part on how much they have been affected by the shock wave. Nininger (1956) reports that all the meteorites they recovered on the plains surrounding the crater show clear Widmanstätten figures with mineralogy typical of iron meteorites. The irons recovered close to the crater up to its rim, on the other hand, show evidence of strong heating that destroyed the Widmanstätten pattern, caused partial melting, recrystallization, and strong deformations (Knox 1970; Axon 1963; Buchwald 1975a).

3. These meteorites can be formed either by disruption of the parent body in the atmosphere followed by separate landing of small fragments or by solid projectile ejecta from the growing crater. Rim specimens (highly shocked and deformed "shrapnel," small in size and without regmaglypts and ablation crust that are characteristic for meteorites) most certainly represent these ejecta. Plain

specimens (moderately or lightly shocked, bigger in size, regular in shape and with regmaglypts and ablation crust) may represent fragments detached from the main body. However, some of the plain fragments (especially those moderately shocked) could be projectile ejecta.

4. *Metallic spheroids*: These tiny objects (mostly a fraction of a millimeter in size) are abundantly distributed within about 8 km from the crater. They were first discovered by Nininger during a survey of the crater region in 1946 (Nininger 1947). After extensive sampling, Nininger estimated that between $4 \cdot 10^6$ kg and $8 \cdot 10^6$ kg of metallic spheroids were distributed in the upper 4 inches of the soils over a region within about 2.5 miles from the rim of Meteor Crater (beyond that limit the amount was too small for adequate measurements). Using these estimates and the concentration of extraterrestrial Ni and Co in these spheroids, Nininger went as far as hypothesizing that the recovered spheroids may be representative of an original deposit of impactor material of around 10^8 kg representing what until then was considered the "lost" impactor mass (Nininger 1956). A similar survey was carried out in 1956 by the Smithsonian Astrophysical Observatory and gave an estimate of about 10^7 kg of small meteoritic debris distributed in the mantle of soil surrounding the crater (Rinehart 1958). On average, metallic spheroids appear to be sorted with distance, with the largest spheroids located on the crater rim and decreasing in size with increasing distance from the rim (Nininger 1956). They also have a rather asymmetric distribution; the highest concentration of metallic spheroids is northeast of the crater rim, while they are rare or almost absent southwest of the rim. The spheroids appear to be enriched by a factor of 2 to 3 in Ni, Co, and Cu compared to the well-known Canyon Diablo irons (Moore et al. 1967). It was this enrichment that drove Nininger to hypothesize that they were vapor condensates of projectile material. As he put it: "I could think of no other way to account for these little droplets, two and a half time as rich in nickel as similar-sized irregular fragments, than that they were condensation droplets from a meteoritic cloud produced by the explosion which Moulton had hypothesized" (Nininger 1973). He connected their distribution with a dispersion of the vaporized impactor by prevailing southwesterly winds in the region. However, Rinehart (1958) pointed out that the spheroids distribution is similar to that of the sizeable Canyon Diablo irons, concluding that the two sets of meteoritic material, large chunks and small spheroids, were dispersed by the same mechanism: the impact event itself (winds could not disperse large chunks). He also suggested that the spherules were possibly formed from impactor melt, not a vapor. His hypothesis was later confirmed by Blau et al. (1973) who pointed to the spheroids' dendritic structure with eutectic infilling as unambiguous evidence that they were formed by solidification from a liquid alloy under non-equilibrium conditions. Kelly et al. (1974) later suggested that Fe depletion was caused by oxidization by atmospheric oxygen during the spheroids' flight away from the impact site. Further confirmation of the solidification from a melt came with the identification of cosmogenic gases in the spheroids, which could not be present if they condensed from a vapor (Leya et al. 2002).

5. *Sluglets*: Nininger identified as "sluglets" irregularly shaped particles that at the lower end are comparable to the metallic spheroids and at the upper end they seem to grade into the regular Canyon Diablo irons. Sluglets appear to make up for a very small component of projectile material.

6. *Shale Balls*: Barringer (1909) defines shale balls as rounder or globular disintegrating masses, up to 30 cm in diameter, of meteoric iron and nickel oxide, many of them containing solid Fe-Ni centers. The chemical analyses indicate that they are like the Canyon Diablo irons except for a small concentration of chlorine which is practically absent in the irons. The presence of chlorine tends to accelerate the oxidation of iron meteorites. Some shale balls also preserve some hints of Widmanstätten figures in their interior (Barringer 1909).

7. *Metallic particles in impactites*: Originally, the name "impactites" was adopted to define silica-glass slag, mostly in the form of little bombs, found in association with impact structures (Spencer 1933). Nininger started to look for similar products around Meteor Crater and quickly found them all around the crater in the form of small, micron- to mm-size bombs in coincidence with metallic spheroids and sluglets (Nininger 1954, 1956). He estimated that in the most heavily impregnated horizon, the amount of this slag ranged around 30 to 100 kg/m^3. These impactite bombs also contained spherules of magnetite enriched in nickel and cobalt, and show a very large range in Ni content, from 6 to 95% (Kelly et al. 1974).

Combined together, these historical materials suggest few important (albeit preliminary) conclusions: 1) at least some impactor fragments broke up from the impacting body and fell in the surrounding plains with minor volume heating, but with ablation crust and regmaglypts typical for meteorites; the total mass of the collected CD meteorites is about $3 \cdot 10^4$ kg; 2) the impact caused melting of a significant fraction of the impactor, which was then distributed over the surrounding plains (at least ~10^7 kg, based on the spheroids); 3) since spheroids indicate melting and not vaporization, material recovered near the crater does not support a hypothesis of massive vaporization of impactor material. However, field data cannot rule out possible vaporization and subsequent dispersion of the vaporized material.

The Fate of the Impactor—Numerical Models

Meteor Crater is not simply the first terrestrial crater officially recognized as an impact structure based on high-pressure quartz polymorphs (Chao et al. 1960, 1962), but it is the first planetary impact event that was modeled numerically (Bjork 1961). The first numerical (two-dimensional) simulation by Bjork (1961) consisted of an iron projectile striking vertically at 30 km/s a target made of tuff. The fate of the projectile seemed to be sealed with the results of this simulation: it was obvious that the impactor would be completely destroyed by the impact explosion and mixed with target material, and no portions of it should be expected to be found intact beneath the crater. One important conclusion of this work was that to create a crater the size of Meteor Crater, assuming a reasonable impact velocity value, would require an impactor close to 10^8 kg in mass, ruling out the lower (less than $2 \cdot 10^7$ kg based solely on recovery of meteoritic material) as well as higher (e.g., 2.2 10^9 kg, estimated by Opik [1961]) limits.

The next numerical modeling study of Meteor Crater (Bryan et al. 1978) assumed an impact velocity range of 11 to 40 km/s, based on estimates by Shoemaker (1977) of Earth-crossing asteroids velocities. They pointed out that since Zel'dovich and Raizer (1967) estimated that the minimum impact velocity required for a meteorite to reach complete vaporization was about 14 km/s, it was very probable that a significant portion of the Canyon Diablo impactor was vaporized in the formation of Meteor Crater. In a detailed study of the formation of Meteor Crater, Roddy et al. (1980) modeled a vertical impact of an iron projectile using two different impact velocities of 25 and 15 km/s, and a mass of $5.1 \cdot 10^7$ kg and $1.4 \cdot 10^8$ kg, respectively, to maintain a constant impact energy of 3.8 Mt (1 Mt = 4.184×10^{15} J). This study also emphasized that peak shock pressure in the projectile and adjacent rock was sufficiently high to result in complete vaporization of the projectile in the fastest impact simulation, where the maximum shock pressure obtained was of the order of 1,000 GPa. The presence of Canyon Diablo meteorites with low or non-existent shock features was then attributed to spallation from the main meteorite during atmospheric passage.

It took about 20 years for the next publication of numerical modeling of the Meteor Crater impact event. In 1999, Schnabel et al. (1999) investigated the fate of the Canyon Diablo impactor by combining numerical modeling with estimates of depth of origination for iron meteorites and metallic spheroids using cosmogenic nuclides. They modeled the Canyon Diablo impact by a spherical iron impactor 30 m in diameter, striking a target made of an 80 m layer of limestone followed by a quartzite basement at 20 and 15 km/s. To estimate the amount of melting in the projectile, Schnabel et al. used experimental data for shock melting of stainless steel (Bass et al. 1990), corresponding to 234 GPa for incipient and 271 GPa for complete melting (slightly lower than experimental data for pure Fe; Bass et al. 1987). Theoretical estimates for Fe, using

the updated ANEOS equation of state (Melosh 2000) and JANAF thermochemical tables (Chase 1998), give slightly higher values, 301 and 380 GPa, respectively (Pierazzo et al. 1997), while the threshold for shock vaporization for Fe are estimated around 850 GPa. Simulation results suggested that a shell in the outer part of the trailing hemisphere of the projectile remained solid and could be the source of the Canyon Diablo meteorites. The shell was estimated to be 1.5 to 2 m thick and to correspond to about 15% of the projectile mass for a 20 km/s impact, increasing to about 5 m thickness (63% of the projectile mass) for a 15 km/s impact.

Thus, early numerical modeling of the projectile fate in the impact confirms the preliminary conclusions of the previous subsection: part of the projectile remains solid, while vaporization is minor.

So far, all of the Canyon Diablo impact simulations have used a coherent object. However, already in his 1909 paper, Barringer suggested that the impactor was a swarm of objects, with a heavy central mass (or masses) responsible for the formation of the crater. This idea was renewed recently by Melosh and Collins (2005). Using a simple model for the fragmentation and dispersion of the impactor (the pancake model; Chyba et al. 1993), they concluded that the Canyon Diablo impactor was disrupted and significantly slowed in the atmosphere. Their estimates, assuming projectile spreading up to 4 initial radii and a surviving fragment of 1.45 10^8 kg (½ the initial mass), indicated that this fragment would have reached the surface with an impact velocity of 12 km/s, releasing about 2.5 Mt of energy. They then explained the lack of significant melting of target rocks at Meteor Crater (Kieffer and Simonds 1980) by the impact velocity being too low to produce significant melting.

METEOR CRATER PROJECTILE— SIZE BEFORE IMPACT

Estimates of the mass of the Canyon Diablo meteoroid have varied widely (see historical sections). Even though over time the estimates have been clustering toward a common value, an iron object around 40–60 m in diameter, its pre-impact, and especially pre-atmospheric, masses are still poorly known. Below we introduce various factors that contribute to the uncertainty in the estimates of the size of the Canyon Diablo impactor. Besides variability due to scaling laws, uncertainties associated with mass and velocity estimates come from factors such as projectile dispersion in the atmosphere, impact angle, target layering and porosity, and water table in the target. We briefly discuss these factors below.

Projectile Size-Velocity and Crater Size—Scaling Laws

Schmidt (1980) used scaling laws derived from centrifuge impact experiments in Ottawa sand to define the energy of formation for Meteor Crater. For his estimates he used the values of apparent crater volume, 0.075 km^3, and

radius, 511 m (from Roddy 1978). His results, expressed in terms of projectile energy instead of projectile mass, are shown in Fig. 1 by dashed lines. The dashed line with V symbols represents crater volume scaling: $E_v(ergs) = 2.59 \cdot 10^{19} U^{0.78}$ (U is impact velocity in cm/s). The dashed curve with R symbols represents crater radius scaling: $E_r(ergs) = 1.33 \cdot 10^{19} U^{0.80}$. Since the velocity range of the centrifuge experiments is 1.3–7 km/s, the values of mass/energy for higher velocities were obtained by a simple extrapolation. Schmidt also determined a lower bound estimate (dashed line in Fig. 1) based on quarter-root scaling at constant mass, by assuming that high-velocity impacts have lower cratering efficiency with more energy transferred into melting and vaporization. Impact velocities higher than 7–8 km/s are still unfeasible in impact cratering laboratory experiments. However, the comparison of modern computer simulations with geological records (Pierazzo et al. 1997; Ivanov 2005) suggests that the scaling laws are valid for high impact velocities at planetary scales as well. Therefore, Schmidt's lower bound is shown mainly for historical reasons.

Current scaling laws (Schmidt and Housen 1987; Holsapple 1993; see also http://keith.aa.washington.edu/crater data/scaling/index.htm) use parameters related to the transient cavity diameter D_{tc}, instead of the final crater. Simple geometrical models (Dence 1973; Grieve and Garvin 1984; Grieve et al. 1989) suggest a volume of 0.094 km³ and a diameter of 876 m (final crater would be 1.25 times larger) as the best estimate for Meteor Crater apparent transient cavity (assuming that depth is a factor of $2^{-1.5}$ smaller than diameter; Dence 1973). Laboratory scaling laws assume a transient cavity depth/diameter ratio of 1:4, which requires an increase of the transient crater diameter to 985 m (about 100 m larger) to maintain the same transient cavity volume (alternatively, the transient crater depth should be smaller). Substituting coefficients for soft rocks (differences in effective material strength are not important for Meteor Crater which is substantially larger than strength dominated craters) and taking into account a depth/diameter ratio of 0.25, we obtain for the transient cavity size:

$$D_{tc} = 0.926 \left(\frac{\rho_{pr}}{\rho_t} \right)^{1/3} U^{0.43} d_{pr}^{0.78} g^{-0.22} \qquad (1)$$

with $D_{tc} = 0.985$ km., or, for the projectile diameter:

$$d_{pr} = 1.1 \left(\frac{\rho_t}{\rho_{pr}} \right)^{0.42} U^{-0.55} D_{tc}^{1.27} g^{0.27} \qquad (2)$$

where g is terrestrial gravity, ρ_{pr} and ρ_t are projectile and target densities, respectively. These scaling laws provide another set of values for the Meteor Crater projectile, where impact into soft rocks gives an order of magnitude smaller projectile mass than impact into sand (Schmidt 1980) for the same impact velocity (Fig. 1, thick black line).
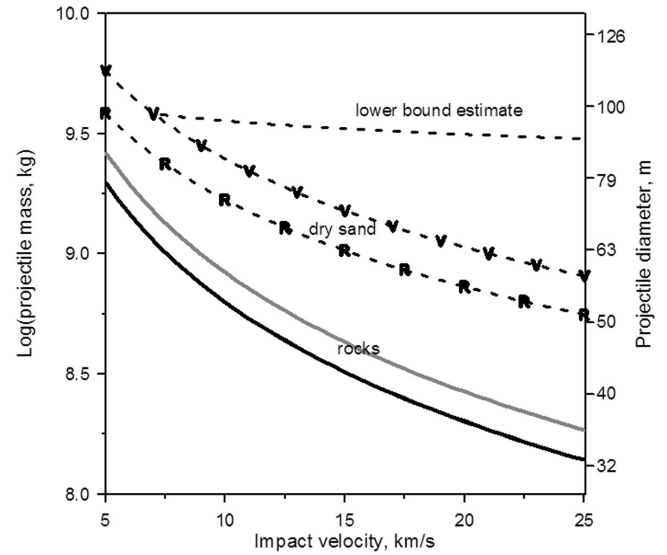

Fig. 1. Iron projectile mass (i.e., size) and velocity needed to produce a simple final crater 1200 m in diameter or/and transient apparent cavity volume of 0.094 km³ in gravity regime. Dashed lines are for Schmidt (1980) estimates, derived from the experiments in dry sand and recalculated from projectile energy to projectile mass and velocity ("V" is for volume scaling, "R" is for crater radius scaling; simple dashed line is the lower bound estimate based on quarter root scaling). The solid lines show more recent Schmidt and Housen (1987) scaling laws for wet soils and rocks; black line: intact projectile; gray line: cluster with dispersion of 3 (corresponding to 27 times lower density).

In our study, we use the scaling results for soft rocks as input values for the projectile mass and velocity used for simulating the Meteor Crater impact.

Scaling Laws for Disrupted and Dispersed Projectiles

The only published set of experimental data for disrupted projectiles is by Schultz and Gault (1985). They conclude that scaling for craters created by dispersed projectiles is essentially the same as for solid projectiles ($\pi_v \sim \pi_2^{-\alpha}$, where $\pi_v = \rho_t V/m_{pr}$ is scaled crater volume) as long as the diameter in the dimensionless parameter $\pi_2 = g d_{pr}/U^2$ is the diameter of the cluster, not the initial projectile size (see Fig. 3 of Schultz and Gault 1985). Those experiments were done in sand and pumice targets; however, we can extrapolate their conclusion to high-velocity impacts into competent rock. The end result is that scaling equations for the impact of clustered projectiles are the same as for solid projectiles (Equations 1 and 2) as long as the cluster density ρ_{cl} and size d_{cl} is used in place of intact projectile values. Assuming a spherical shape for the cluster (as observed in the experiments; Schultz and Gault 1985), cluster properties can then be connected to those of the intact projectile by using a coefficient of projectile dispersion $C_d = d_{cl}/d_{pr}$, that is the ratio of cluster diameter to projectile diameter. Then cluster density is $\rho_{cl} = \rho_{pr} C_d^{-3}$, cluster diameter $d_{cl} = C_d d_{pr}$, and the transient crater and projectile

diameters are:

$$D_{tc} = 0.926 \left(\frac{\rho_{pr}}{\rho_t}\right)^{1/3} U^{0.43} d_{pr}^{0.78} g^{-0.22} C_d^{-0.22} \quad (3)$$

$$d_{pr} = 1.1 \left(\frac{\rho_t}{\rho_{pr}}\right)^{0.42} U^{-0.55} D_{tc}^{1.27} g^{0.27} C_d^{0.26} \quad (4)$$

The experimental data of Schultz and Gault (1985) describe a wide range of projectile dispersions, C_d (from 1 to >20). While the cratering efficiency is almost constant for C_d values up to 10, the crater shape is more sensitive to a projectile dispersion. Moderately dispersed projectiles (tight clusters, $C_d < 3$) produce regular craters similar to those formed by a solid impactor, but with lower displaced target mass. Open clusters ($3 < C_d < 10$) create craters that are wider and shallower, grading into irregular clusters of separated shallow craters when $C_d > 10$ (Schultz and Gault 1985).

A crucial characteristic of Meteor Crater is that its shape and depth/diameter ratio are typical of simple craters (as measured on the Moon; Pike 1977), suggesting that projectile dispersion of Canyon Diablo should be less than 2–3. The mass of the cluster at the surface for a maximum dispersion of about 3 is shown in Fig.1 by a thick gray line. This mass does not differ substantially (due to the weak dependence on dispersion in Equation 4) from estimates for a solid impactor, shown by the thick black line.

Impact Obliquity and Other Factors

Impact angle will introduce further uncertainty in these scaling-based estimates. The standard assumption is that for a natural impact crater size scales with impact angle in the same way laboratory impacts do: $D_{tc} \sim \sin\theta^{0.43}$ (Chapman and McKinnon 1986). This implies that the projectile size necessary to form Meteor Crater increases with decreasing impact angle as $\sin \theta^{-0.55}$. However, it was shown that in terms of crater volume a high-velocity moderately oblique impact has almost the same efficiency as a vertical impact (Ivanov and Artemieva 2002). This suggests that the projectile size depends on the impact angle much more weakly than $\sin \theta^{-0.55}$ (this assumption is for impact angles at least >30° from the surface; a grazing impact would not even create a crater). Given the regular shape of Meteor Crater and its ejecta, we cannot expect a very low angle of impact. Assuming an impact range of 30°–90° the overall uncertainty in projectile size due the angle of impact is around 20%, much less than uncertainties described above.

Another factor that may influence crater formation is the target's porosity. Pressure decays faster in porous targets compared to crystalline ones because of the additional irreversible work needed to crush void space. Thus, smaller craters and less highly shocked materials are expected in a porous target for the same projectile size and velocity (Love et al. 1993; Wünnemann et al. 2005); vice versa, a larger

projectile is needed to create the same crater in porous rocks. However, typical porosity for local materials is not very high; in the case of Meteor Crater the maximum estimated porosity is about 25% for the Coconino formation; see Roddy 1980).

The formation of steam upon pressure release in water-saturated targets enhances the crater cavity growth and produce an increase in crater volume compared to dry target rocks. Moreover, fluids are likely to change the mode and yield of impact induced failure in rocks (Kieffer and Simonds 1980). Recent high-velocity impact experiments have confirmed the increase of crater volume in wet sandstone (e.g., Kenkmann et al. 2006). Water may also substantially influence ejecta (melt, in particular) dispersion (Artemieva 2007).

We will consider the influence of all the factors discussed above in a follow up paper. Here we will concentrate on projectile disruption/dispersion in atmosphere.

NUMERICAL MODELS FOR ATMOSPHERIC ENTRY

Atmospheric entry can be described by simplified differential equations for 1) *a point mass without disruption* (McKinley 1961), or with a simplified treatment of disruption, either 2) *the separated fragments model* (Passey and Melosh 1980; Artemieva and Shuvalov 1996, 2001), or 3) *the pancake model* (Chyba et al. 1993). The alternative to the simplified approach is to use 4) *full-scale hydrodynamic models* in which the projectile is treated as a strengthless continuous body (Ahrens et al. 1994; Takata et al. 1994; Crawford et al. 1995), as a body with some kind of strength (Ivanov and Melosh 1994), or as a cloud of fragments (Svetsov et al. 1995). Since the internal properties of comets and asteroids are poorly known, simplified approaches are competitive with more comprehensive hydrodynamic models because they allow us to investigate systematically a wide range of input parameters over a short period of time. However, as we show, depending on the approximation used, the final results (fragments' masses, their velocities) may differ by an order of magnitude. Under the same initial conditions the no-disruption regime will provide maximum pre-impact velocity and minimum pre-atmospheric mass, while the pancake model with infinite projectile spreading will provide minimum pre-impact velocity and maximum pre-atmospheric mass.

Separated Fragments (SF) Model and Pancake Model

Even though the hypothesis of the disruption of an impactor traveling through the atmosphere can be traced back to Barringer's early studies of Meteor Crater, the actual importance of atmospheric disruption for small bodies (up to a few hundred meters in diameter) was realized only much later. The first analytical study, based on observations of terrestrial crater strewn fields, was carried out by Passey and

Melosh (1980). They describe the evolution of a disrupted body as a two-stage process: 1) a strong but short interaction of the fragments immediately after the disruption, followed by 2) the motion of individual fragments. This analytical model was translated into a numerical model by Artemieva and Shuvalov (1996, 2001), and was named the Separate Fragments (SF) model. The SF model has been applied to a wide range of impactor (pre-atmospheric) masses by Bland and Artemieva (2003, 2006).

The SF model considers successive fragmentations and ablations of individual fragments (where the number of fragments, N, ranges from 1, at the start, and may be as large as a billion at the end). A meteoroid is disrupted into a pair of fragments whenever the dynamic loading exceeds its strength, which depends on the meteoroid type and size. Fragment mass and direction of separation (the two fragments move away from each other in opposite directions) are defined at random. Immediately after the breakup, fragments tend to have a higher strength than the parent body, but can be disrupted again into a new pair later on, when the dynamic loading exceeds the fragments' strength. The differential equations of motion (Melosh [1989], p. 206–207) are solved for each individual fragment, with an additional equation describing separation between the two broken up fragments (Artemieva and Shuvalov 1996, 2001). The model is most applicable for bodies smaller than a few meters in diameter; for larger bodies the basic assumption of "separation" among fragments becomes quickly invalid. In this case, a dense cloud of fragments tends to decelerate as a cloud, not as individual particles. In other words, the gas velocity is not negligible compared to the fragments velocities (see Artemieva and Shuvalov [2001] for details).

Another way to describe the atmospheric disruption and dispersion of impactors is via the pancake model (Zahnle 1992; Chyba et al. 1993; Hills and Goda 1993; Collins et al. 2005). This simple analytical model treats the disrupted meteoroid as a deformable continuous fluid. The model was used to describe comet-like and stone meteoroids, while application to irons is questionable. The use of this model introduces many uncertainties and "ad hoc" choices, the most important being the maximum allowed radius of pancaking. In the original model (Zahnle 1992), there were no restrictions on the growth of the pancake radius. However, this simplification leads to unrealistically thin and wide projectiles and to extremely low final velocities (essentially, deceleration is inversely proportional to the projectile's thickness). Numerical models (Ivanov et al. 1992; Ahrens et al. 1994; Takata et al. 1994; Crawford et al. 1995) carried out around the same time that the pancake model was developed (i.e., the time of the collision of comet Shoemaker-Levy 9 with Jupiter) clearly showed that although flattening ("pancaking") is a typical behavior of disrupted projectiles, it is mostly restricted to a flattening factor of 1.7–2.3. Further, widening is arrested by the growth of Kelvin-Helmholtz (K-H) and Rayleigh-Taylor (R-T) instabilities and the resulting projectile fragmentation into smaller pieces. This kind of behavior was observed in early laboratory experiments of the breakup of liquid droplets by gas streams (Ranger and Nichols 1970) and is reproduced in more recent numerical simulations (Shuvalov et al. 1999; Shuvalov and Artemieva 2002). However, commonly used restrictions on the maximum spread of the object (above 2) are purely artificial. Different choices of the object's maximum spread can lead to substantially different results even for identical initial conditions. It should also be kept in mind that the pancake model does not describe the object behavior after maximum spreading is reached (would the object keep its shape and mass or would only some part of its mass reach the surface, while the rest fragments and disappears in the atmosphere?). We assume that the whole mass reaches the surface, while Melosh and Collins (2005) assumed that only half of the mass reached the surface to make Meteor Crater. Hydrodynamic simulation can provide some constraints on this estimate; however, an accurate determination is difficult to make, due to many other unknowns (exact projectile shape, strength, internal structure, etc.). Still, the pancake model (with the maximum pancake radius recommended above) may be successfully used for weak cometary-like projectiles, which are disrupted into small fragments and are deformed more uniformly.

We have reproduced the pancake model by adding minor modifications to the SF model. This was possible because the pancake model utilizes the same equations of motion for an intact body used by the SF model (Melosh 1989, p. 206–207), with only an additional equation for spreading (Chyba et al. 1993).

Obviously, neither the pancake model nor the SF model are realistic models for the evolution of the Canyon Diablo projectile. An accurate reproduction of this event requires the application of full-scale hydrodynamic modeling. However, we choose to show results of both the SF and pancake models, as they are widely used (especially the pancake model) in the community, and to compare them (when used properly) with the more realistic hydrodynamic model.

Full-Scale Hydrodynamic Model (SOVA)

The best solution for an accurate investigation of impactor disruption in the atmosphere is through direct numerical modeling of the atmospheric entry. This is a computationally expensive numerical procedure to carry out in systematic studies, considering that small bodies must be followed through distances exceeding by far their diameter (in the case of the Canyon Diablo projectile—50 m versus 20–50 km). This causes obvious computation cost versus resolution issues, especially considering that internal properties of incoming objects (shape, strength, porosity, homogeneity) are still poorly known. This approach, therefore, can only be used for investigating a few test cases, after a more systematic investigation has been carried out with the simpler models.

To model the atmospheric deceleration of a projectile, initial stage of the crater formation (compression and excavation), and high-velocity material ejection, we use the three-dimensional (3D) hydrocode SOVA (Shuvalov 1999) coupled to ANEOS-derived equation of state tables for the materials involved in the simulations. SOVA is a two-step Eulerian code that can model multidimensional, multi-material, large deformation, strong shock wave physics. It includes a general treatment of viscosity for modeling viscous flow with Newtonian or Bingham rheology, while the implementation of the Rigid-Plastic Model (RPM; Dienes and Walsh 1970; Shuvalov and Dypvik 2004) allows us to mimic plastic behavior of the projectile. In addition, SOVA can describe the motion of solid/melt particles in an evolving ejecta-gas-vapor plume and their momentum-energy exchange using two-phase hydrodynamics, which takes into account both individual particle characteristics (mass, density, shape) and their collective behavior (momentum and energy exchange with surrounding gas).

PROJECTILE MODIFICATION DURING ATMOSPHERIC ENTRY

It is well known from astronomical records, geological observations, and numerical modeling, that meteorites with size larger than few tens of cm are subjected to intense disruption in the Earth's atmospheres. The Canyon Diablo projectile indeed followed this fate, as witnessed by the numerous meteorites that landed separately from the main (cratering) mass on the plains surrounding the crater. Therefore, the determination of the pre-atmospheric mass of the Meteor Crater projectile is not a simple task.

Initial Conditions and Meteoroid Strength

In our model we use an iron projectile with a typical iron density of 7800 kg/m^3, an initial velocity of 18 km/s, and impact angle of 45°. We also used an ablation coefficient of 0.07 s^2/km^2, in agreement with theoretical calculations by ReVelle and Rajan (1989) and with observations of the U.S. Prairie Network fireballs identified as irons (ReVelle and Ceplecha 1994). The projectile diameter varies over a wide range (see below).

The most uncertain of all of the meteoroid properties, and unfortunately a crucial property as well, is strength. Strength can be estimated using two independent methods: 1) astronomical observations of meteorite entry (Ceplecha et al. 2000), where the strength is defined by velocity and height at the moment of disruption; 2) direct measurements on meteorite samples in the laboratory (Knox 1970). The latter method give accurate results for small meteoroids (usually mm-sized) already altered by atmospheric entry; however, dynamic strength of larger impactors is believed to be much lower than laboratory measurements of small meteorites. The

former method tends to provide a less accurate but more realistic dynamic strength; however, while some information is available for chondrite- and comet-like objects (Ceplecha et al. 2000), no data seem to be available for iron objects at this time.

Early strength measurements of forged iron meteorite materials (see Knox [1970], for details) are in the range 370–440 MPa (both in tension and compression). Knox (1970) measured the compressive yield strength of three meteorites (Canyon Diablo, Odessa, and Brenham) using specimens 4 mm and 8 mm in length. While Canyon Diablo and Brenham have similar strength of about 410 MPa at 0.4% of plastic strain, Odessa is approximately 25% weaker. The largest iron specimen ever measured in the laboratory is a 1 kg sample of the Sikhote-Aline iron shower, which gave a tensile strength of 44 MPa (Yavnel 1963; Krinov 1974), about an order of magnitude smaller than the smaller Canyon Diablo and Brenham irons.

In general, the strength of the parent bodies is substantially lower than the meteorites that derived from them due to the presence of fractures and faults. The average strength of a body of mass m can be defined by a Weibull (1951) statistics: $\sigma = \sigma_0(m_0/m)^\alpha$, where m_0 and σ_0 are the mass and the strength values of the known sample, α is a constant that varies with projectile type over the range 0.05–0.25 (smaller values for homogeneous materials, higher values for strongly non-homogeneous materials with internal cracks and faults). The initial strength of impacting bodies, including Canyon Diablo, is poorly constrained. We use the value of α = 0.07, which gives reasonable results for the well-studied Sikhote-Aline iron meteorite shower (see Artemieva and Shuvalov 2001). Disruption occurs when dynamic pressure exceeds the tensile strength, σ. For a realistic size range of the Meteor Crater projectile, this results in first disruption occurring at an altitude of about 10–20 km.

No-Disruption and Pancake Models Output

The lower bound for the initial mass of the Canyon Diablo projectile can be determined by modeling its atmospheric penetration with no disruption, that is, by solving the standard set of differential equations for atmospheric entry (e.g., see Melosh [1989], pp. 206–207). With this approach, for any given projectile size we see rather small changes in mass and velocity from the initial values (Fig. 2, black squares), usually no more than 3–4%. Without disruption, an iron asteroid with initial diameter as small as 40 m can produce a crater the size of Meteor Crater. On the other hand, this scenario sounds rather unrealistic for two reasons: 1) it requires an unusually high value of projectile internal strength of ~150 MPa, which is more than 3 times higher than the strength of a laboratory sample weighing 1 kg; 2) it does not agree with the abundance of small meteorites (fragments of the same asteroid) found near Meteor Crater.

If we use the pancake model, we find major differences from the intact object approach. In Fig. 2, black circles show final masses and velocities for a Canyon Diablo projectile using the pancake model with a flattening factor of 2. While mass losses are not much higher than without disruption, the decrease in pre-impact velocities from the initial 18 km/s is substantial: the smallest projectile decelerates to 15 km/s, the largest—to 16 km/s. The decreased impact velocity calls for slightly larger projectiles than in the no-disruption case, around 42–43 m, to form Meteor Crater (i.e., to keep the same impact energy). The most dramatic change in impact velocities occur if we allow flattening corresponding to a cross section diameter increase of up to 4 times the initial diameter (black diamonds in Fig. 2). In this case, the projectile velocity drops to 7 km/s for the smallest projectile and to 12 km/s for the largest. These results are in good agreement with the results of Melosh and Collins (2005), who considered a similar flattening. In this extreme case, to create Meteor Crater, the pre-atmospheric projectile size should be ~52 m with a final impact velocity (at the surface) of ~11 km/s.

Obviously, meteoroid strength can affect the pancake model results. Gray diamonds in Fig. 2 correspond to the same 4 times flattening parameter, but to a 3 times higher projectile strength. As expected, a higher strength leads to a lower altitude of disruption and a higher final velocity. However, this parameter does not seem to affect the final outcome of the model as much as the flattening parameter. Therefore, the pancake model can be efficiently used to estimate atmospheric effects on an impactor, but the pancaking parameter must be chosen very carefully. *It is important to keep in mind that pancaking values much above 2 do not appear to fit either current numerical models nor common sense.*

SF Model—Distribution of Fragments Over Size and Velocity

The pancake model does imitate the meteoroid's deformation during the atmospheric entry, but does not predict the final size and velocity distribution of the disrupted fragments. To investigate the effect of fragmentation during entry of the Canyon Diablo meteoroid, we applied the SF model to an iron projectile 30 m in diameter ($1.67 \cdot 10^8$ kg). This projectile is a bit too small to produce Meteor Crater, but the modeling demonstrates principal features of the SF model and its final outputs.

As discussed above, the strength of a meteoroid's fragment may depend on its size. Moreover, each new fragment may have its own unique strength. For this reason, for every new fragment with mass m_f we adopt a random value within a normal statistical distribution of strength around the Weibull (1951) average value for m_f with deviation of 1–2 (see Artemieva and Shuvalov [2001] for details). For this study, we use the measured mass and strength values of
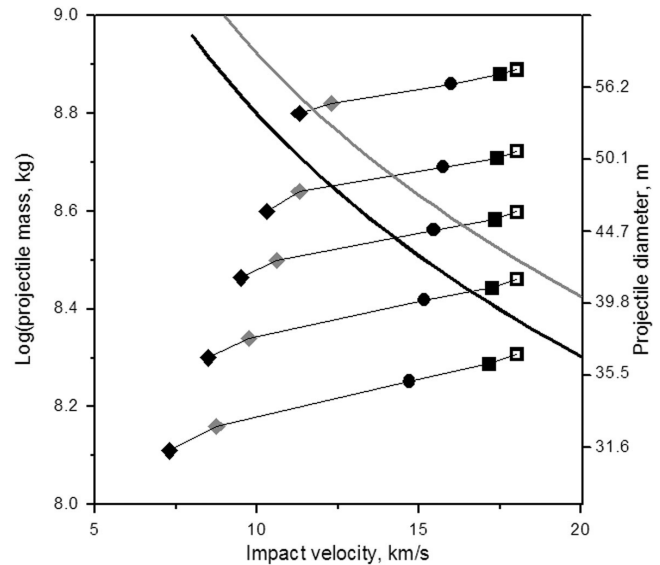

Fig. 2. Pre-atmospheric (open squares) and pre-impact (black and gray symbols) projectile mass versus impact velocity for different pancake model assumptions. Thick black and gray lines are the same as in Fig. 1 and show mass-velocity coupling for the Meteor Crater. Open squares show initial velocity of 18 km/s and various initial sizes—from 36 m to 57 m. Black squares are for non-disrupting (but ablating) meteoroid; black circles show pancaking to 2 initial radii; black and gray diamonds—pancaking to 4 initial radii with gray for 3 times higher strength of the entering body. Thin lines connect projectiles with the same initial size. While the model with disruption or with pancaking up to two initial radii allows to create the Meteor Crater by a projectile ~40 m in diameter with final velocity of about 16 km/s, pancaking to 4 initial radii demands a projectile ~50 m in diameter with final velocity less than 11 km/s.

the Sikhote-Aline sample, that is $m_0 = 1$ kg and $\sigma_0 = 44$ MPa, and $\alpha = 0.07$. For different runs with the same initial conditions, the final results, in terms of size-frequency distribution of the fragments and their velocities, may differ substantially depending on the random choice of strength: in some cases a very "strong" fragment survives the flight and can thus create a large crater, in others only small fragments (<1,000 kg) are generated, which strike the surface with lower velocity, thus corresponding to a "loose" or "weak" projectile. Figure 3 shows the final velocity versus mass for fragments larger than 10^4 kg. Gray symbols are used to represent the "strong" projectile case, i.e., the case in which a few dominant fragments with mass of $4 \times 6 \times 10^7$ kg strike the surface with a final velocity around 16 km/s. Black symbols are used to represent the "weak" projectile case, in which all fragments are smaller than 8×10^6 kg and the final velocity of the largest fragments is less than 14 km/s. The smallest fragments modeled decelerate to 4 km/s (the disruption produce even smaller fragments, down to cm in size, which strike the surface with terminal velocity, but we excluded them from our simulations). On average, there is a direct correlation between final velocity and final fragment mass. However, due to multiple fragmentation some small fragments can reach the
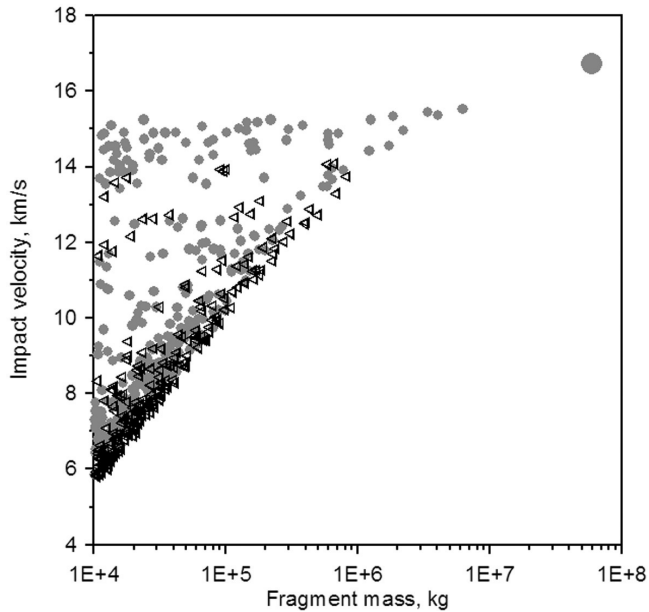
Fig. 3. Mass-velocity distribution of separated fragments, which may create the Meteor Crater. Black triangles show the case of a "weak" projectile with millions of small fragments. Gray circles show the case of a "strong" projectile with one dominant fragment (in this example, with a mass of $8 \cdot 10^7$ kg) and thousands of smaller ($<10^7$ kg) fragments. For each mass in the figure, the lowest velocity value corresponds to the fragment separation in the upper atmosphere, while higher velocities correspond to fragments separated from the main body at lower altitudes.
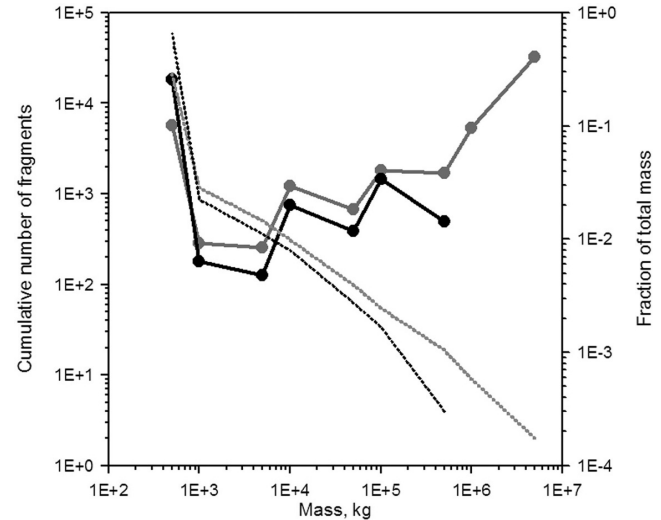

Fig. 4. Cumulative number of fragments (dashed lines and left axis) and fraction of their mass in total mass (solid lines and right axis). Gray lines and symbols represent the case of a strong projectile, black ones represent a weak one. Although total pre-impact masses are similar in both cases, 40% of the mass of the strong projectile are in two large pieces ($M_{fr} > 5 \cdot 10^6$ kg), while 30% of the weak projectile are in small ($M_{fr} < 500$ kg) pieces. The total mass distributed among intermediate fragments (1000 kg $< M_{fr} < 10^5$ kg) is similar in both cases.

surface with unusually high velocities, up to 16 km/s. These are fragments that separated from larger fragments late in the trajectory and did not experience substantial deceleration.

Figure 4 shows the cumulative number of fragments for the "strong" and the "weak" projectile cases. In the weak projectile case, the total number of small (500–1000 kg) fragments is double that for the strong projectile case (not to mention billions of smaller pieces). Interestingly, the cumulative mass of intermediate size fragments (1000–10,0000 kg) is similar for the two cases, whereas the mass distributed among smaller fragments (<1000 kg) is about 30% of the total mass for the weak projectile, and only 10% for the strong projectile.

The projected crater distribution created by the disrupted meteoroid in the two cases is shown in Fig. 5. The left side of Fig. 5 corresponds to the "strong" projectile case from Fig. 3, the right side corresponds to the "weak" projectile case. Because the fragments separation is smaller than the overlap of the craters formed by their impact, the craters will not be distinguished individually, but they will combine to form a single comprehensive structure. In the case of smaller entry masses (early breakup and wider fragments separation), this distribution would have created a strewn field, where the craters are all separated. Typically, the largest crater in terrestrial crater strewn fields does not exceed 300 m (Artemieva and Bland 2003). Final crater sizes in the two

cases can be estimated using scaling laws (Schmidt and Housen 1987). In the strong projectile case (Fig. 5, left) the estimated diameter of the largest crater is only slightly less than 1 km and the final crater will be slightly larger due to the addition of smaller impacts. In the weak projectile case (right) all craters are less than 300 m in diameter, but their overlap may ultimately lead to a km-size crater. However, based on experimental data on impact of disrupted fragments (Schultz and Gault 1985), the resulting crater will be substantially shallower than if it was formed by a single fragment. In both cases, the maximum dispersion (distance between separate craters) is about 400 m. This value does not depend on the amount of fragments and/or their sizes, but is mainly defined by the atmospheric density profile and the height of disruption (usually of about 10–15 km) (see Passey and Melosh [1980] and Artemieva and Shuvalov [2001]).

Based on these results, it appears that even though used beyond its upper limit of applicability (5 m in diameter object, Artemieva and Shuvalov [2001]) the SF model produces reasonable results for the "strong" projectile (in this case the total amount of fragments is modest and the whole process is defined by a few largest fragments). The same model does not work well for large numbers of fragments (e.g., a very weak impactor). In this case the fragments move like a "swarm," and not only the individual particle properties are important, but also their collective mass and velocity. While it is still possible to neglect direct collisions between particles, the gas between particles is not still anymore; it has a final velocity. The end result is a lower overall drag and a higher final
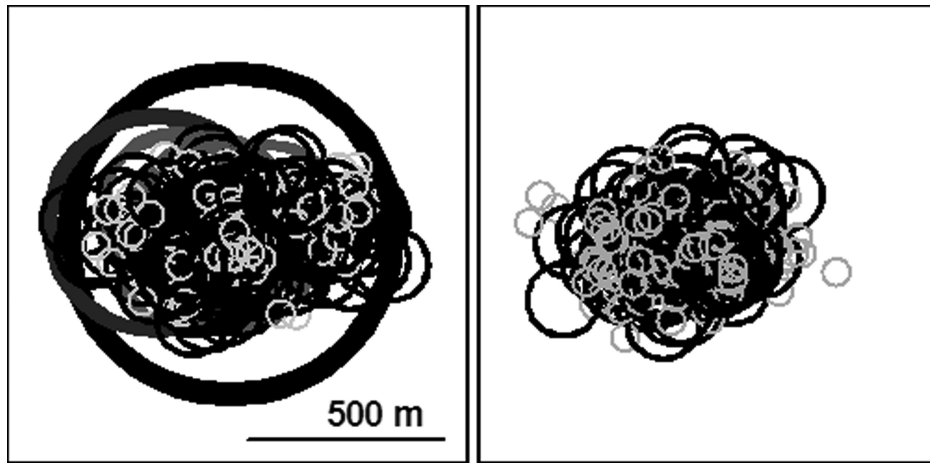
Fig. 5. Strewn fields created by projectile swarms shown in Fig. 3. Left: strong projectile case, with the final main crater just a bit smaller than the meteor. Right: weak projectile case, in which all craters are smaller than 100 m, but the final crater diameter may be comparable with that of Meteor Crater.

collective velocity of the swarm. The application of the SF model to the Canyon Diablo impactor (tens of meters in diameter) is not adequate and may introduce significant errors, especially in pre-impact velocity. For a more accurate study of the breakup of the Canyon Diablo impactor, we must use a hydrodynamic simulation of the projectile penetration in the atmosphere.

Hydrodynamic Modeling of Atmospheric Entry—Continuous Body

We use SOVA in Cartesian three-dimensions to model gas flow around an iron projectile entering the Earth's atmosphere at 18 km/s. In the simulations, we adopt a standard spherical shape for the impactor and a resolution of 20 cells per projectile radius. This is not a "real" asteroid shape. However, any asymmetry in asteroid shape leads to its quick rotation during atmospheric entry and the resulting "average" shape is close to a sphere. Strong asymmetries or pre-existing faults are also conducive to meteoroid disruption and separation in the very early stages of atmospheric penetration. Therefore, our results represent an idealized situation which may underestimate projectile deformation and disruption. To model the equivalent of an initial trajectory at 45° from the vertical, we stretch the standard distribution of density in the Earth's atmosphere by a factor of $\sqrt{2}$. Test runs using a strengthless body show a quick and unrealistic disruption (i.e., strong deformations and dispersion of continuum into isolated droplets) of the entering body. We use the rigid-plastic approximation to describe a body with standard strength that takes into account iron hardening with pressure increase and softening with temperature increase (with zero strength at melting point; Johnson and Cook 1983). Figures 6A–6E show a few snapshots of the simulation. The initially spherical body becomes strongly deformed around heights of 6 km, its central part (experiencing maximum

dynamic loading) thins out until it is finally disrupted into a few large pieces (only one is visible in Fig. 6C). Below 4 km altitude, the dynamic pressures exceeds by far the material strength and the meteoroid quickly changes its shape and transforms into an irregular jet of fragments, melt droplets, and vapor. Apparently, the scenario of disruption (i.e., thinning in the central part of the body and jet formation) does not depend on the initial body shape. Figures 6F–H show the final irregular jet of an initially cylindrical body in three dimensions, i.e., cross sections along the flow are combined with cross sections across the flow. During atmospheric entry about 25% of the meteoroid initial mass is lost while the velocity decreases by about 10%. Similar results can be obtained using the pancake model with the assumption of a maximum flattening of about 2, corresponding to a cross section diameter increase of up to 2 times the initial impactor diameter (see Fig. 2).

The hydrodynamic approximation treats the body as a continuum and does not include disruption into individual particles. This is an adequate approximation for bodies subjected to ductile deformation (such as very weak cometary bodies) and/or for bodies disrupted into tiny dust-like fragments of similar size. Iron impactors may be subjected to brittle fragmentation with a wide range of fragments' sizes. It is thus necessary to investigate the importance of the motion of individual fragments within a tight swarm.

Hydrodynamic Modeling—Swarm of Particles

In the previous section, we modeled the entering projectile as a continuum. However, this approach does not allow to resolve the fate of numerous small fragments. In this section, we use an expanded version of SOVA to model the flow of a particle-gas mixture; i.e., to describe the motion of small undeformable solid particles in the gas flow. To describe the motion of a tight swarm of particles, we assume
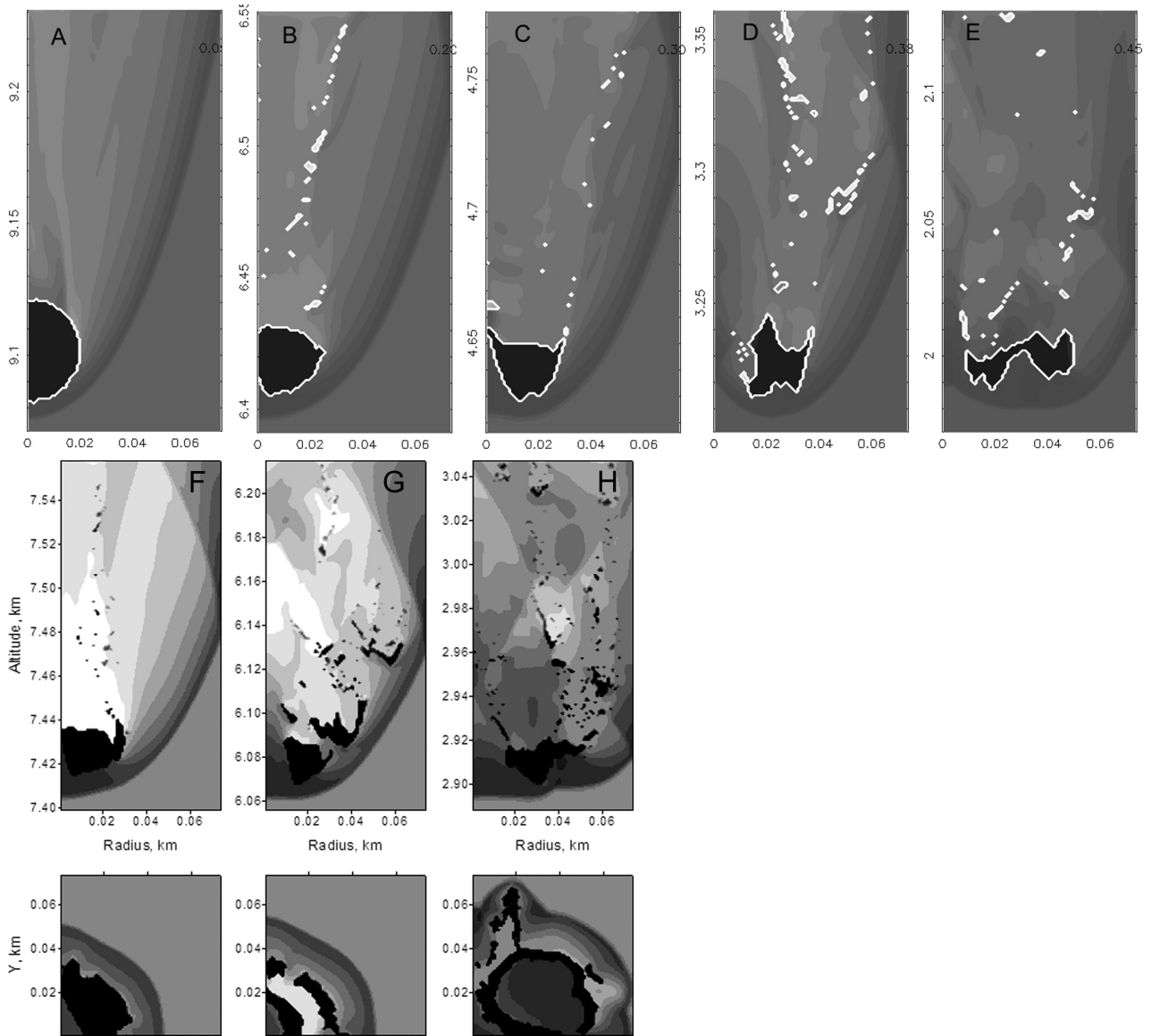
Fig. 6. Snapshots of hydrodynamic modeling of atmospheric entry. Gray shading describes atmospheric density; black with white boundaries shows the iron meteorite. The simulation is symmetric around the direction of motion, thus only half of the flow is shown (the other half being its mirror image). The initial spherical meteorite radius is 20 m (plate A), it flattens to 1.5 of its initial size (plates B and C), and then is disrupted into a large "leading" piece and many smaller fragments in its wake (plate D and E). Plates F–H show disruption of a similar cylindrical body (cross sections along the flow are at the top and across the flow at the bottom).

immediate disruption of an entering body into fragments of different size with an initial velocity of $V_0 = 18$ km/s along the trajectory at 10 km from the surface (the first fragmentation usually occurs at much higher altitudes, around 30–50 km, however, final catastrophic fragmentations of large iron bodies are observed below 10 km—see Krinov 1974). This scenario requires the initialization of more parameters than the models described above. Not only is the initial projectile mass important, but also its initial dispersion (right after disruption), the particles' lateral velocity (perpendicular to the trajectory), and the particles' size-frequency distribution (SFD).

In our approach, we use a SFD that is characteristic for the disruption of solid material under dynamic loading, represented by a power law of the type: $N_{>M} = (M/M_{max})^{-b}$, where $N_{>M}$ is number of fragments with mass larger than M, and the largest fragment mass M_{max} and exponent b are two more input parameters to be determined. Typical values of b for multiple fragmentation are around 1, with values >1 occasionally observed near impact craters (see Melosh [1989], p. 91). Here we used the value of 1.2 to avoid numerous very small fragments. To obtain the total projectile mass with $b < 1$ the SFD must be continued to infinitely small masses. However, for $b > 1$ the SFD must be limited to some

critical size to reach the same total mass; in our model this sizes is ~1 mm. Eventually, most of the mass of the swarm is between 0.001 and 0.1 of the total projectile mass (the former corresponding to the weak projectile's case of the SF model, the latter to the strong projectile's case).

The small lateral velocity component is proportional to the square root of the density ratio ρ_a/ρ_{pr}, according to the aerodynamic breakup theory (Passey and Melosh 1980; Melosh 1989, p. 207–209). For typical disruption altitudes of 10–20 km, atmospheric density ρ_a is around $4\cdot10^{-4} \div 8\cdot10^{-5}$ g/cm^3; since meteoroid density ρ_{pr} is 7800 kg/m^3, the lateral velocity could be up to $(0.003 \div 0.001)\,V_0$, or $50 \div 20$ m/s. The initial radius of the swarm can vary; we consider that reasonable values of the ratio of the swarm to intact-body radius for the Canyon Diablo case (dispersion C_d, similar to the definition of Schultz and Gault 1985) are between 1.1 (extremely tight swarm) and 3 (moderately tight swarm).

However, we begin with two end-member examples, which are not directly representative of the Canyon Diablo case (one being clearly too small, the other too strong), but that represent the extremes in projectile behavior during its motion through the atmosphere. Furthermore, these two end-member cases demonstrate the applicability of the models used and the connection between SF model (on the low end of projectile masses) and hydrodynamic model (on the upper end).

The first example, shown in Fig. 7, is the simulation of atmospheric entry of a relatively small iron body with total pre-atmospheric mass of $1.3\cdot10^6$ kg (corresponding to a diameter of 6.8 m before disruption) with an unrealistically large dispersion (according to experimental data) $C_d = 13$ (normally allowed, for example, by the pancake model), which creates an initial swarm 88 m in diameter and fragment diameters varying from 12 cm to 2 m (five particle bins in total, corresponding to fragment masses between 5.5×10^{-6} and 0.025 projectile masses). About 0.05 s after disruption, fragments are well separated along the trajectory according to their size with the largest fragments moving ahead of the smallest. At this time the total spread of the swarm reaches 200 m, and keeps increasing, becoming 700 m 0.1s later. Although the velocity of 10 cm-sized particles is still far from terminal velocity, at the end of the simulation they lost approximately half of the entry velocity, while the largest lost less than 7% (Fig. 7). The velocities of individual particles coincide with the results of the simplified SF analytical model (open symbols in Fig.7). Because the separation occurs quickly, meteoroids of this size (and with similar initial dispersion) can be described correctly by the SF approximation. Therefore, the use of the hydrodynamic modeling in this case is not an efficient approach, given the significant computer time required to run the hydrodynamic simulation.

The situation is dramatically if we consider a tight ($C_d = 1.18$) and massive ($M_{tot} = 1.3\cdot10^9$ kg, $D = 68$ m) swarm of particles with disruption occurring at the same altitude of 10 km and with a SFD similar to the previous case. In this case, the swarm moves like an intact solid body within a single shock wave (Fig. 8, left plate). At an altitude of 5 km (Fig. 8, central plate) some separation across the trajectory occurs, and the average density of the impactor drops below 3000 kg/m^3. In contrast to the previous example, however, all particles move with similar velocities, ~17.4 km/s. Close to the surface (Fig. 8, right plate), as the atmosphere becomes denser, some fragments detach from the swarm and decelerate as individual objects (these will land far from the crater), while the largest fragments move ahead of the main swarm, creating a higher density precursor. Even with this separation of fragments, we can still treat this object as a tight swarm (according to the terminology of Schultz and Gault 1985), since dispersion is about 2 and the average density is about 700 kg/m^3. The swarm still contains 82% of the initial mass and ends up striking the surface with a velocity of 15.8 km/s. Although the final (near the surface) velocity and mass look similar to the continuum hydrodynamic simulations and to the pancake model output, a fundamental difference is the much lower final density of the projectile than in these models. Contrary to the SF model, all fragments within the swarm have similar final velocities, independent on their size.

The two extreme cases show that depending on the fragments' initial mass and dispersion, full separation may or may not occur during atmospheric passage. Figure 9 summarizes the results of simulations with various initial (pre-atmospheric) conditions, including various degrees of dispersion immediately after disruption and various initial SFD, but with constant height of disruption. Pre-atmospheric masses (shown by black symbols for different initial masses) range from $1.65\cdot10^8$ to $4.45\cdot10^9$ kg (i.e., projectile diameter— from 34 to 102 m), dispersions range from 1.2 to 5, and mass of the largest fragment in the swarm ranges from 2.5% to 0.0025% of the initial meteoroid mass. Final velocities and masses are shown with open symbols. The results indicate that the influence of SFD and initial fragments' random distribution is usually minor (symbols within the dashed circle in Fig. 9 are very close together). The trends for initial masses and dispersions are rather obvious: A larger dispersion results in a smaller near-surface mass and a lower near-surface velocity (Fig. 9). However, the bigger impactors appear to be less sensitive to the value of dispersion: the smallest impactor of $1.65\cdot10^8$ kg with dispersion of 2.5 loses 80% of its mass and 30% of its initial velocity, while larger impactor of $1.3\cdot10^9$ kg with same dispersion loses only 30% of its pre-atmospheric mass and 10% of its initial velocity.

Preatmospheric masses around 1.0–$1.3\cdot10^9$ kg and modest initial dispersions around 1.2–2.5 provide the best fit with scaling laws. During the entry the body loses approximately half of its mass due to fragments' separation (mechanical ablation) and reaches the surface with a velocity of 15–16 km/s. Final dispersion is less than 3, suggesting that this swarm should create a regular simple crater. In the experiments (Fig. 15 in Schultz and Gault 1985) a higher value of dispersion (and lower impact velocity) can still provide the
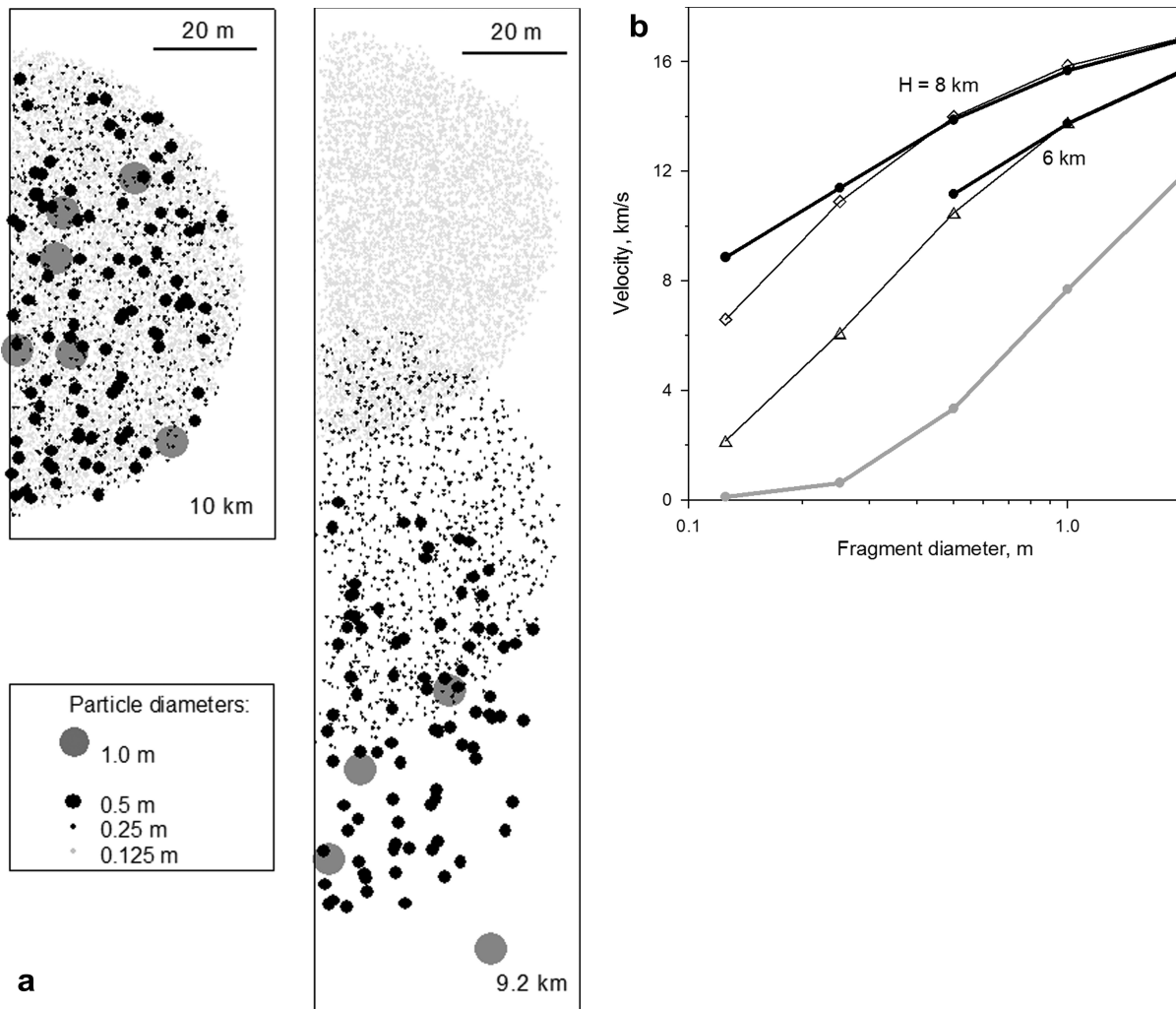
Fig. 7. a) Separation of a small (6.8 m diameter) and strongly dispersed projectile (dispersion factor of 13) occurs quickly after disruption. Large gray circles are for fragments 1 m in diameter (the largest fragment in this run is twice this size, but is not in the central cross section of the flow); large black circles represents fragments 0.5 m in diameter; black dots are for fragments 0.5 m in diameter; and gray dots represent the smallest fragments, 12.5 cm in diameter. Initially (at an altitude of 10 km, left upper plate) particles are distributed within a sphere 88 m in diameter and have the same velocity of 18 km/s. At an altitude of 9.2 km (right plate), i.e., 0.044 s later, the swarm is separated into 3 distinct sub-swarms with the largest fragments moving ahead of the smallest. b) Particle velocities as a function of altitude (only 3 classes of the largest particles are shown for an altitude of 6 km, as the smallest are far behind the leading fragments and out of the mesh). Curves with open symbols show fragments' velocities according to SF model and are in a good agreement with SOVA calculations. Thick gray line is final (near-surface) velocity, calculated with SF model: the smallest fragments reach the surface with terminal velocity, intermediate ones lost more than a half of the entry velocity, and the largest have high enough velocities to create well-separated craters (strewn field).

standard crater morphology. Thus, overall we should not expect a shallow crater for a dispersion of 3.

The fate of fragments that were detached from the swarm and landed separately is defined by their size and altitude of separation. Our estimates show that fragments larger than 70 cm land within the growing crater, although with low velocities of 0.3–1.5 km/s. This means that they may be strongly affected by the cratering process. Smaller pieces reach the plains outside the crater with terminal velocities, which depend on their size (<300 m/s), after a substantial time delay (>20s, i.e., together with distal crater ejecta). According to our model, these fragments should be distributed within a

~400 m wide strewn filed—projection of the projectile trajectory on the surface. As such projectile-rich stripe is not observed near Meteor Crater, smaller fragments were strongly affected by the ejecta or were re-distributed afterwards.

The best model approach to describe an atmospheric entry of the meteor-like projectiles is still not achieved. This "perfect" model should combine the hydrodynamic description of the largest pieces (as in section Hydrodynamic Modeling of Atmospheric Entry—Continuous Body) with a dusty flow approach for the smallest fragments (as in section Hydrodynamic Modeling—Swarm of Particles). Realistic strength model for iron meteorites may be of crucial
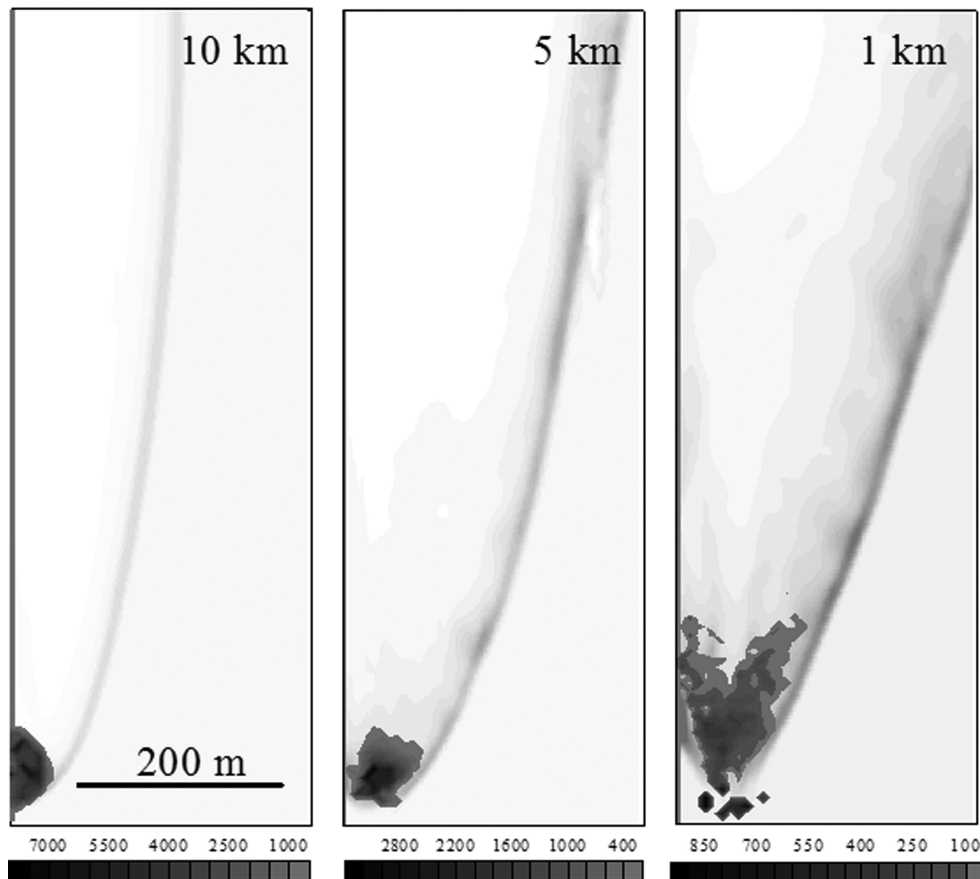
Fig. 8. Simulation for a large (68 m in diameter), tight (C_d = 1.18) projectile swarm. The three images show the projectile at 10 (height of disruption), 5 and 1 km from the surface. Although this simulation uses the same particles size as in Fig. 7, the smaller dispersion and larger amount of particles makes it impossible to show them individually. Thus, the gray scale in the figure shows the density within the swarm Although an increase of initial swarm radius and, hence, substantial decrease of its density occurs over time, there is no clear "separation" among particles of different size: all particles move within the same shock wave with similar velocities. This motion is similar to the flight of a solid body (Fig. 6). However, close to the surface (e.g., image corresponding to 1 km from surface) the largest fragments (densest region, almost black in the figure) are slightly (at most tens of m) ahead of the main swarm. Overall, the final swarm is tight enough to create a single crater with normal morphology.

importance. The radiation transfer and ablation of high-velocity fragments should be taken into account as well.

CONCLUSIONS

Meteor Crater is one of the best studied terrestrial impact structures, yet there are still many puzzling questions about its creation. While pioneering modeling work on impact cratering started with studies of Meteor Crater in the early 1900s, the last 25 yr have seen little modeling work on this famous crater. We present results of the first part of a modeling study of the formation of Meteor Crater aimed at investigating projectile entry and fragmentation. Melting and material ejection during crater formation will be addressed in a following paper.

All previous numerical studies of the Meteor Crater impact event have modeled the projectile as a coherent object. However, already in his 1909 paper, Barringer suggested that the impactor was a swarm of objects, with a heavy central mass (or masses) responsible for the formation of the crater.

This idea was renewed recently by Melosh and Collins (2005). They used the pancake model (Chyba et al. 1993) to estimate the disruption and slowing experienced by the projectile during its motion through the atmosphere. They concluded that a surviving fragment would have reached the surface with an impact velocity of 12 km/s, too low to produce significant melting of target rocks. In this work, we present a detailed study of projectile motion in the atmosphere through the application of the SF model and full scale hydrodynamic simulations to the Canyon Diablo impact event, and compare our model results to available data and to the pancake model (Melosh and Collins 2005) to characterize the early stage of the Canyon Diablo impact event.

Our findings can be summarized as follow:

1. The pancake model is a simple and efficient instrument to estimate impact velocities for meteorites subjected to disruption. The best fit with more sophisticated models is for a flattening parameter of 1.5–2. Higher values (e.g., 4, used by Melosh and Collins [2005]) are inconsistent with
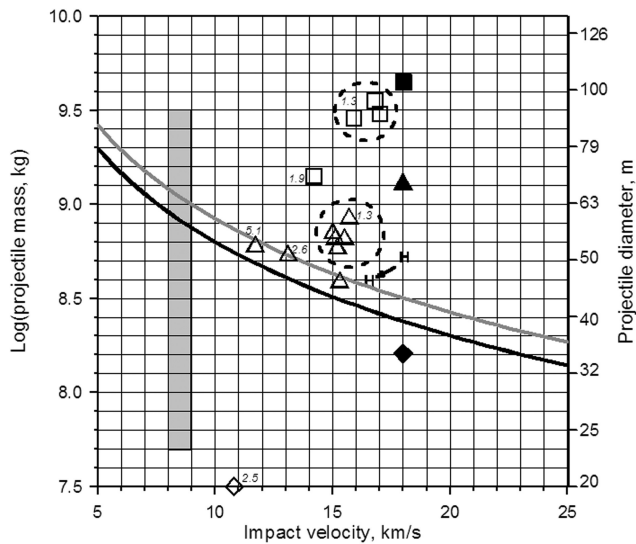
Fig. 9. As in Fig. 1, black and gray lines show mass-velocity combination needed to create Meteor Crater. Gray rectangle is for Moulton's estimates (1929). Different symbols represent the various outputs of hydrodynamic modeling of the swarm: squares are for the largest impactor (diameter of an intact body, D = 103 m), triangles for the medium impactor (D = 68 m), and diamonds for the smallest impactor (D = 34 m). The symbol "*H*" represents hydrodynamic simulations of a continuum solid deformable body. Black symbols represent the pre-atmospheric masses and velocities (all are 18 km/s). Open symbols are for various initial dispersions (numbers near the symbols) and various initial SFD. Variants with the same initial dispersion but with different SFD give similar final results and are enclosed by dashed circles.

hydrodynamic models and result in lower impact velocities than predicted by more sophisticated modeling.

2. It is difficult to estimate precisely the pre-atmospheric Canyon Diablo projectile size. In this size range both of the commonly used analytical models (SF and pancake) are incorrect. The SF model is only appropriate for smaller bodies where fragments are really separated; the pancake model is appropriate only for the weak bodies that are deformed and disrupted more uniformly. The results from more sophisticated numerical models depend strongly on unconstrained parameters, such as meteoroid strength, criteria of disruption, distribution of fragments with size, and initial dispersion of the fragments' swarm.

3. The best way to model the Canyon Diablo atmospheric entry is with a full-scale hydrodynamic modeling with an appropriate strength model. However, this approach does not properly resolve the fate of small fragments. Alternatively, small fragments may be described in the frame of two-phase hydrodynamics. As a temporary acceptable solution, we suggest that the Meteor Crater projectile be modeled as a continuum if the main goal of the modeling is the crater formation itself (lost details about small fragments do not influence the process). If

the main goal of the model is material distribution on the plains, a two-phase approach is more suitable.

4. Based on our current knowledge of meteoroids in space and their relation to meteorites, we can bracket the pre-atmospheric mass of the Meteor Crater projectile between $4 \cdot 10^8$ and $1.2 \cdot 10^9$ kg, equivalent to a spherical body 46 to 66 m in diameter (the lower limit came from hydrodynamic modeling for a solid body, while the upper limit is for a heavily fragmented swarm). Our modeling indicates that the impactor that created Meteor Crater retained 30–70% of the original meteoroid mass. The main loss mechanism is mechanical ablation and gross fragmentation (again, the lower limit is for ductile deformations of a solid body, the upper limit is for a swarm). Even in the case of a tight swarm of particles, small fragments can separate from the crater-forming swarm and land on the plains (tens of km away from the crater) as individual meteorites.

5. A large mass loss of the original meteoroid appears inconsistent with ^{3}He and cosmogenic nuclides investigations of Canyon Diablo meteorites and spherules, which pointed to their origin from a 1–2 m thick outer shell of the projectile. This brings us back to the still outstanding problem of the projectile material deficiency near Meteor Crater. If all projectile material identified so far came from the outer shell, where is the rest?

6. Assuming a pre-atmospheric velocity of ~18 km/s (average for Earth crossing asteroids), the most probable impact velocity at the surface for a tight swarm seems to be 15 km/s or higher. A loose swarm of projectile fragments (and hence, lower impact velocity) is inconsistent with the Meteor Crater structure. However, lower impact velocities cannot be ruled out totally, since we cannot exclude that the velocity of the Canyon Diablo impactor was close to the lower limit (down to 11 km/s) for Earth-crossing asteroids.

Editorial Handling—Dr. Uwe Reimold

REFERENCES

Ahrens T. J., Takata T., and O'Keefe J. D. 1994. Impact of comet Shoemaker-Levy 9 on Jupiter. *Geophysical Research Letters* 21: 1087–1090.

Artemieva N. 2007. Possible reasons of shock melt deficiency in the Bosumtwi drill cores. *Meteoritics & Planetary Science* 42:883–894.

Artemieva N. and Bland P. 2003. Crater fields on Venus, Earth and Mars (abstract #1319). 34th Lunar and Planetary Science Conference.

Artemieva N. and Shuvalov V. 1996. Interaction of shock waves during the passage of a disrupted meteoroid through the atmosphere. *Shock Waves* 5:359–367.

Artemieva N. and Shuvalov V. 2001. Motion of a fragmented meteoroid through the planetary atmosphere. *Journal of Geophysical Research* 106:3297–3309.

Axon H. J. 1963. Destruction of the Widmanstätten structure in iron meteorites by laboratory heat treatment. *Nature* 197:1291.

Barringer D. M. 1909. *Meteor Crater (formerly called Coon Mountain or Coon Butte), in northern central Arizona*. Read before National Academy of Sciences, Princeton University. Privately printed.

Bass J. D., Svendsen B., and Ahrens T. J. 1987. The temperature of shock compressed iron. In *High-pressure research in mineral physics*, edited by Manghnani M. H. and Syono Y. Tokyo: Terra Scientific, and Washington, D.C., American Geophysical Union. pp. 393–402.

Bass J. D., Ahrens T. J., Abelson J. R., and Hua T. 1990. Shock temperature measurements in metals—New results for an Fe alloy. *Journal of Geophysical Research* 95:21767–21776.

Bjork R. L. 1961. Analysis of the formation of Meteor Crater, Arizona: A preliminary report. *Journal of Geophysical Research* 66(10):3379–3387.

Bland P. and Artemieva N. 2003. The impact rate of 10^2—10^{12} kg objects at the Earth's surface. *Nature* 424:288–291.

Bland P. and Artemieva N. 2006. The rate of small impacts on Earth. *Meteoritics & Planetary Science* 41:607–631.

Blau P. J., Axon H. J., and Goldstein J. I. 1973. Investigation of the Canyon Diablo metallic spheroids and their relationship to the breakup of the Canyon Diablo meteorite. *Journal of Geophysical Research* 78(2):363–374.

Bryan J. B., Burton D. E., Cunningham M. E., and Lettis Jr. A. 1978. A two-dimensional computer simulation of hypervelocity impact cratering: Some preliminary results for Meteor Crater, Arizona. Proceedings, 9th Lunar and Planetary Science Conference. pp. 3931–3964.

Buchwald V. F. 1975a. *Handbook of iron meteorites*, vol. 1. Berkeley: University of California Press. pp. 125–136.

Buchwald V. F. 1975b. *Handbook of iron meteorites*, vol. 3. Berkeley: University of California Press. pp. 937–942.

Ceplecha Z., Borovička, and Spurný P. 2000. Dynamical behaviour of meteoroids in the atmosphere derived from very precise photographic records. *Astronomy & Astrophysics* 357:1114–1122.

Chao E. C. T., Shoemaker E. M., and Madsen B. M. 1960. First natural occurrence of coesite. *Science* 132:220–222.

Chao E. C. T., Fahey J. J., Littler J., and Milton D. J. 1962. Stishovite, SiO_2, a very high pressure new mineral from Meteor Crater, Arizona. *Journal of Geophysical Research* 67:419–421.

Chapman C. R. and McKinnon W. B. 1986. Cratering of planetary satellites. In *Satellites*, edited by Burns J. A. and Matthews M. S. Tucson: The University of Arizona Press. pp. 492–580.

Chase M. W., ed. 1998. *NIST-JANAF thermochemical tables*, 4th ed. J. Phis. Chem. Ref. Data, Monograph No. 9. Woodbury, NY: American Chemical Society. 1963 p.

Chyba C. F., Thomas P. J., and Zahnle K. J. 1993. The 1908 Tunguska explosion: Atmospheric disruption of a stony asteroid. *Nature* 361:40–44.

Collins G. S., Melosh H. J., and Marcus R. A. 2005. Earth impact effects program: A web-based computer program for calculating the regional environmental consequences of a meteoroid impact on Earth. *Meteoritics & Planetary Science* 40:817–840.

Crawford D. A., Boslough M. B., Trucano T. G., and Robinson A. C. 1995. Numerical modeling of Shoemaker-Levy 9 impacts as a framework for intepreting observations. *Geophysical Research Letters* 22:1821–1824.

Dence M. R. 1973. Dimensional analysis of impact structures. *Meteoritics* 8:343–344.

Dienes J. K. and Walsh J. M. 1970. Theory of impact: Some general principles and the method of Eulerian codes. In *High-velocity impact phenomena*, edited by Kinslow R. New York: Academic Press. 579 p.

Grieve R. A. F. and Garvin J. B. 1984. A geometric model for excavation and modification at terrestrial simple impact craters. *Journal of Geophysical Research* 89:11,561–11,572.

Grieve R. A. F., Garvin J. B., Coderre J. M., and Rupert J. 1989. Test of a geometric model for the modification stage of simple impact crater development. *Meteoritics* 24:83–88.

Hills J. G. and Goda M. P. 1993. The fragmentation of small asteroids in the atmosphere. *Astronomy Journal* 105:1114–1144.

Hörz F., Mittlefehldt D. W., See T. H., and Galindo C. 2002 Petrographic studies of the impact melts from Meteor Crater, Arizona, USA. *Meteoritics & Planetary Science* 37:501–531.

Holsapple K. A. 1993. The scaling of impact processes in planetary sciences. *Annual Reviews of Earth and Planetary Science* 21: 333–373.

Ivanov B. 2005. Numerical modeling of the largest terrestrial meteorite craters. *Solar System Research* 39:381–409.

Ivanov B. A. and Melosh H. J. 1994. Dynamic fragmentation of a comet (abstract). 25th Lunar and Planetary Science Conference. pp. 598–599.

Ivanov B. and Artemieva N. 2002. Numerical modeling of the formation of large impact craters. In: *Catastrophic events and mass extinctions: Impact and beyond*, edited by Koeberl C. and MacLeod K. G. GSA Special Paper 356. Boulder: Geological Society of America. pp. 619–630.

Ivanov B. A., Nemchinov I. V., Svetsov V. V., Provalov A. A., Khazins V. M., and Phillips R. J. 1992. Impact cratering on Venus: Physical and mechanical models. *Journal of Geophysical Research* 97(E10):16,167–16,183.

Johnson G. R. and Cook W. H. 1983. A constitutive model and data for metals subjected to large strains, high strain rates and high temperatures. Proceedings, 7th International Symposium on Ballistics. pp. 541–547.

Kelly W. R., Holdsworth E., and Moore C. B. 1974. The chemical composition of metallic spheroids and metallic particles within impactite from Barringer Meteorite Crater, Arizona. *Geochimica et Cosmochimica Acta* 88:533–543.

Kenkmann T., Thoma K., Deutsch A. and the MEMIN-team. 2006. Hypervelocity impact into dry and wet sandstone (abstract #1587). 37th Lunar and Planetary Science Conference. CD-ROM.

Kieffer S. W. and Simonds C. H. 1980. The role of volatiles and lithology in the impact cratering process. *Reviews of Geophysics & Space Physics* 18:143–181.

Knox R. Jr. 1970. The yield strength of meteoritic iron. *Meteoritics* 5:63–74.

Kring D. 2007. Guidebook to the geology of Barringer Meteorite Crater (a.k.a. Meteor Crater). LPI Contribution 1355. Houston: Lunar and Planetary Institute. 154 p. Available online at http://www.lpi.usra.edu/publications/books/barringer_crater_guidebook/

Krinov E. L. 1974. Fragmentation of the Sikhote-Alin meteoritic body. *Meteoritics* 9:255–262.

Leya I., Wieler R., Ma P., Schnabel C., and Herzog G. F. 2002. Pre-atmospheric depths and thermal histories of Canyon Diablo spheroids. *Meteoritics & Planetary Science* 37:1015–1025.

Love S. G., Hörz F., and Brownlee D. E. 1993. Target porosity effects in impact cratering and collisional disruption. *Icarus* 105:216-224.

McKinley D. W. R. 1961. *Meteor science and engineering*. New York: McGraw-Hill. 309 p.

Melosh H. J. 1989. *Impact cratering: A geologic process*. New York: Oxford University Press. 245 p.

Melosh H. J. 2000. A new and improved equation of state for impact computations (abstract #1903). 31st Lunar and Planetary Science Conference. CD-ROM.

Melosh H. J., and Collins G. S. 2005. Meteor Crater formed by low-velocity impact. *Nature* 434:157.

Merrill G. P. 1908. The Meteor Crater of Canyon Diablo, Arizona; its history, origin and associated meteoric irons. *Smithsonian Institute Miscellaneous Collections* 50:461–498.

Moore C. B., Birrell P. J., and Lewis C. F. 1967. Variations in the chemical and mineralogical composition of rim and plains specimens of the Cañon Diablo meteorite. *Geochimica et Cosmochimica Acta* 31:1885–1892.

Moulton F. R. 1929. *Second report*. Mimeograph copy at Lowell Observatory Library, Flagstaff, Arizona, USA.

Nininger H. H. 1947. Adventures in a magnetic search for meteorites. *Popular Astronomy* 55:273–275.

Nininger H. H. 1954. Impactite slag at Barringer Crater. *American Journal of Science*. pp. 285–286.

Nininger H. H. 1956. *Arizona's meteorite crater. Past—present—future*. Denver, CO: American Meteorite Laboratory. 232 p.

Nininger H. H. 1973. *Find a falling star*. Eriksson P. S. Pub. 254 p.

Nishiizumi K., Kohl C. P., Shoemaker E. M., Arnold J. R., Klein J., Fink D., and Middleton R. 1991. In situ ^{10}Be-^{25}Al exposure ages at Meteor Crater, Arizona. *Geochimica et Cosmochimica Acta* 55:2699–2703.

Opik 1961. *Notes on the theory of impact craters*. Proceedings, Geophys Lab—Lawrence Rad. Lab. Crat. Symp., edited by Nordyke M. D. UCRL-6438 Part II: S1-S28.

Passey Q. R. and Melosh H. J. 1980. Effects of atmospheric breakup on crater field formation. *Icarus* 42:211–233.

Phillips F. M., Zreda M. G., Smith S. S., Elmore D., Kubik P. W., Dorn R. I., and Roddy D. J. 1991. Age and geomorphic history of Meteor Crater, Arizona, from cosmogenic ^{36}Cl and ^{14}C in rock varnish. *Geochimica et Cosmochimica Acta* 55:2695–2698.

Pierazzo E., Vickery A. M., and Melosh H. J. 1997. A re-evaluation of impact melt production. *Icarus* 127:408–423.

Pike R. J. 1976. Crater dimensions from Apollo data and supplemental sources. *The Moon* 15:463–477.

Pike R. J. 1977. Size-dependence in the shape of fresh impact craters on the moon. In *Impact and explosion cratering*, edited by Roddy D. J., Pepin R. O., and Merril R. B. New York: Pergamon Press. pp. 489–510.

Ranger A. A. and Nichols J. A. 1970. Shape and surrounding flow field of a drop in high-speed gas stream. *AIAA Journal* 8:1720–1722.

ReVelle D. O. and Rajan R. S. 1980. Evaluation of initial properties of iron meteoroids using terrestrial crater signatures (abstract). 20th Lunar and Planetary Science Conference. pp. 896–897.

ReVelle D. O. and Ceplecha Z. 1994. Analysis of identified iron meteoroids: Possible relation with M-type Earth-crossing asteroids? *Astronomy and Astrophysics* 292:330–336.

Rinehart J. S. 1958. Distribution of meteoritic debris about the Arizona meteorite crater. *Smithsonian Contributions to Astrophysics* 2:145–159.

Roddy D. J., Boyce J. M., Colton G. W., and Dial A. L. 1975. Meteor Crater Arizona, rim drilling with thickness, structural uplift, diameter, depth, volume, and mass-balance calculations. Proceedings, 6th Lunar Science Conference. pp. 2621–2644.

Roddy D. J., Schuster S. H., Kreyenhagen K. N., and Orphal D. L. 1980. Computer code simulations of the formation of Meteor

Crater, Arizona: Calculations MC-1 and MC-2. Proceedings, 11th Lunar and Planetary Science Conference. pp. 2275–2308.

Schmidt R. M. 1980. Meteor Crater: Energy of formation—implications of centrifuge scaling. Proceedings, 11th Lunar and Planetary Science Conference. pp. 2099–2128.

Schmidt R. M. and Housen K. R. 1987. Some recent advances in the scaling of impact and explosion cratering. *International Journal of Impact Engineering* 5:543–560.

Schnabel C., Pierazzo E., Xue S., Herzog G. F., Masarik J., Creewell R. G., di Tada M. L., Liu K., and Fifield L. K. 1999. Shock melting of the Canyon Diablo impactor: Constraints from nickel-59 contents and numerical modeling. *Science* 285:85–88.

Schultz P. H. and Gault D. E. 1985. Clustered impacts—Experiments and implications. *Journal of Geophysical Research* 90:3701–3732.

Shoemaker E. M. 1963. Impact mechanics at Meteor Crater, Arizona. In *The Moon, meteorites and comets*, edited by Middlehurst B. M. and Kuiper G. P. Chicago: University of Chicago Press. pp. 301–336.

Shoemaker E. M. 1977. Why study impact craters? In *Impact and explosion cratering*, edited by Roddy D. J., Pepin R. O., and Merril R. B. New York: Pergamon Press. pp. 1–10.

Shuvalov V. V. 1999. Multi-dimensional hydrodynamic code SOVA for interfacial flows: Application to thermal layer effect. *Shock Waves* 9:381–390.

Shuvalov V. V. and Artemieva N. A. 2002. Numerical modeling of Tunguska-like impacts. *Planetary & Space Science* 50:181–192.

Shuvalov V. V. and Dypvik H. 2004. Ejecta formation and crater development of the Mjølnir impact. *Meteoritics & Planetary Science* 39:467–479.

Shuvalov V. V., Artemieva N. A., and Kosarev I. B. 1999. 3D hydrodynamic code SOVA for multimaterial flows, application to Shoemaker-Levy 9 comet impact problem. *International Journal of Impact Engineering* 23:847–858.

Spencer L. J. 1933. Meteoric iron and silica-glass from the meteorite craters of Henbury (Central Australia) and Wabar (Arabia). *Mineralogical Magazine* 23:387–404.

Sutton S. R. 1985. Thermoluminescence measurements on shock-metamorphosed sandstone and dolomite from Meteor Crater, Arizona: 2. Thermoluminescence age of Meteor Crater. *Journal of Geophysical Research* 90:3690–3700.

Svetsov V. V., Nemchinov I. V., and Teterev A. V. 1995. Disintegration of large meteoroids in Earth's atmospheres: Numerical models. *Icarus* 116:131–153.

Takata T., O'Keefe J. D., Ahrens T. J., and Orton G. S. 1994. Comet Shoemaker-Levy 9: Impact on Jupiter and plume evolution. *Icarus* 109:3–19.

Weibull W. A. 1951. A statistical distribution function of wide applicability. *Journal of Applied Mechanics* 18:140–147.

Wünnemann K., Collins G. S., and Melosh H. J. 2005. A strain-based porosity model for use in hydrocode simulations of impacts and implications for transient crater growth in porous targets. *Icarus* 180:514–527.

Yavnel' A. A. 1963. Mechanical properties of the Sikhote-Alin meteorite. In *The Sikhote-Aloin Iron meteorite shower*, vol. 2. Moscow: USSR Academy of Science. pp. 362–371. In Russian.

Zahnle K. 1992. Airburst origin of dark shadows on Venus. *Journal of Geophysical Research* 97:10,243–10,255.

Zel'dovich Ya.B. and Razier Yu.P. 1967. *Physics of shock waves and high-temperature hydrodynamic phenomena*, edited by Hayes W. D. and Probstein R. F. New York: Academic Press. 916 p.